ISSN 1330-3651 (Print), ISSN 1848-6339 (Online)
UDC/UDK [681.5.09:629.78.05]:519.876.5

DESIGN AND ANALYSIS OF AN ACTIVE CONTROL PLATFORM FOR WORKING MACHINE ON SPACECRAFT

Yun-Feng Wang, Wei Cheng

Original scientific paper
The micro-vibration produced by reaction wheel assembly (RWA) and other working machines is the dominating reason to descend the pointing accuracy and the image quality of high-precise cameras in spacecraft. In the low damped space environment the micro-vibration decays too slow to keep the performance of the systems. For attenuating the effects of micro-vibration, an active control platform is presented in this study, together with its structural design and control mechanism. Based on the finite element method (FEM) and the properties of piezoelectric material, dynamic model of control platform is developed. In modal space, dynamic model reduction is performed for controller design, and then the periodic output feedback (POF) method is employed to develop the active control system. Simulation is studied under the condition of three random disturbances applying to the centroid of assumed RWA. The results show that the amplitudes of the sensors' responses are decreased more than 20 dB for applying active control with the voltages (≤50V) acted on the eight actuators within the PZT threshold. It can be concluded that this controlling platform can attenuate the disturbances from micro-vibration effectively.

Keywords: *reaction wheel assembly (RWA), active control, finite element model, periodic output feedback (POF), simulation*

Projekt i analiza aktivne upravljačke platforme za radni stroj na svemirskoj letjelici

Izvorni znanstveni članak
Mikro-vibracije koje proizvode sklop zamašnjaka - reaction wheel assembly (RWA) i drugi radni strojevi predstavljaju glavni razlog smanjenja točnosti i kvalitete slike visoko preciznih kamera u svemirskoj letjelici. U okruženju niske vlage u svemiru mikro-vibracije se suviše sporo gube da bi se održalo funkcioniranje sustava. U svrhu smanjenja učinaka mikro-vibracija u ovom se radu predstavlja aktivna upravljačka platforma, njezin konstrukcijski projekt i upravljački mehanizam. Dinamički model upravljačke platforme razvijen je na temelju metode konačnih elemenata (FEM) i svojstava piezoelektričnog materijala. U modalnom prostoru izvršena je redukcija dinamičkog modela u projekt upravljača, a zatim je primijenjena periodic output feedback (POF) metoda za razvoj aktivnog upravljačkog sustava. Simulacija se analizirala u uvjetima tri proizvoljna poremećaja na težištu pretpostavljenog RWA. Rezultati pokazuju da se amplitude reakcija senzora smanjuju više od 20 dB kod primjene aktivnog upravljanja uz napon (≤50V) na osam aktuatora unutar PZT praga. Može se zaključiti da ta upravljačka platforma može učinkovito oslabiti smetnje nastale mikro-vibracijama.

Ključne riječi: *aktivno upravljanje, model konačnih elemenata, periodična izlazna povratna veza (POF), simulacija, sklop zamašnjaka (RWA)*

1 Introduction

Reaction wheel assembly (RWA) and control moment gyroscopes (CMGs) used for attitude control and pointing at scientific targets are important equipment in spacecrafts and satellites. They control the states of spacecrafts and satellites by promoting momentum exchange between the plant and spinning machines, whereas harmful disturbances as result of micro-vibrations would emerge when machines are working. These disturbances would keep for a long time in the low damped space environment and degrade the pointing precision of sensitive equipment such as antennas and cameras. As passive damping limits the amplification at resonance but tends to reduce the high frequency attenuation of the isolation system [1], active control is studied to relieve the effect of such disturbances.

Y. C. Yiu [2] presents the shape memory alloy (SMA) actuators using thermal control to isolate the vibration in spacecraft, but those actuators need a long time to respond to changes in 10 ÷ 50 Hz range. Piezoelectric materials, as the most commonly used active materials in many mechanical and vibration-control systems, have advantages such as high stiffness, fast response, low power consumption, light weight, and easy implementation [3]. Wu Dafang [4] has studied the active vibration control of flexible cantilever beam using PZT actuators by employing independent mode space control method, and the experiment controlling the first-order and second-order modes' vibrations yields excellent controlling effect. B. Bandyopadhyay and T. C. Manjunath [5] develop the dynamic model of smart cantilever beam based on the piezoelectric theory and the finite element method (FEM). The periodic output feedback (POF) method [6], fast output sampling (FOS) method [7], and robust decentralized fast output sampling (RDFOS) feedback control techniques are designed and applied to restraining the vibration of smart cantilever [8]. In these methods the quality feedback to controller is just the output of system, thus they are convenient for implementation. Hanagud [9] discusses the concept of piezoelectric intelligent structure and presents the active control strategy based on the optimal control methods. D. Kamesh [10] designs an active controlling platform used to isolate the vibration of rotary machines in satellites and spacecrafts. It has a good flexibility to control the vibration on low frequency range (0 ÷ 60 Hz). Passive vibration isolation has been studied experimentally by mounting the RWA on low frequency isolation system and comparing the measured disturbances with the disturbances generated from the RWA without the isolator [1].

Zhou Wei Yong [11] employs the Newton–Euler method to develop an analytical model of the reaction wheel assembly (RWA) and the test system, which is then used to model and analyse the micro-vibrations emitted by the RWA, due to the static and dynamic imbalance of the flywheel. Based on that model an intelligent vibration isolation platform for RWA is designed and subject to analysis, with the gyroscopic effect of flywheel taken into consideration [12].

In this paper, an active control platform is presented in Section 2 for attenuating the micro-vibration arising from RWA or CMGs. The structural dynamic model is developed with piezoelectric ceramics as actuators and sensors based on the Euler-Bernoulli beam theory in Section 3. Modal analysis for the platform is carried out and the results are compared with those calculated by ANSYS to validate the model, based on which this finite element model is adjusted for designing the active controller in Section 4. The control system has been developed using the Periodic Output Feedback (POF) method and the simulation has been studied under the condition of random disturbances in Section 5. Section 6 will conclude the performance of this platform.

2 Structure of active control platform

The active control platform in Fig1 contains a load board, four piezoelectric folded-beams, and a base. The disturbance source, especially the RWA, is fixed on the load board. Piezoelectric folded beams with piezoelectric patches glued on their surfaces as sensors and actuators are orthogonal to each other and they are the primary components of control platform, which is shown in Fig 2. They can measure the vibration level of disturbances from the source and generate control forces to attenuate vibration under the commands of control-system. The base is the connector between the platform and the plant (satellite or spacecraft).

Like other isolator's design, this active control platform should support the objects with sufficient static stiffness and strength and also to provide the smallest possible dynamic stiffness [10].

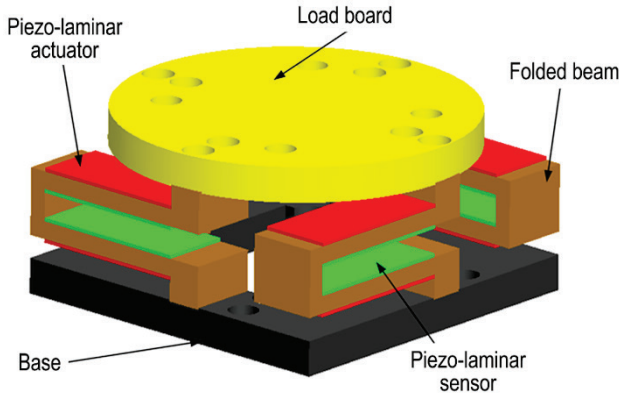

Figure 1 The structure of active control platform

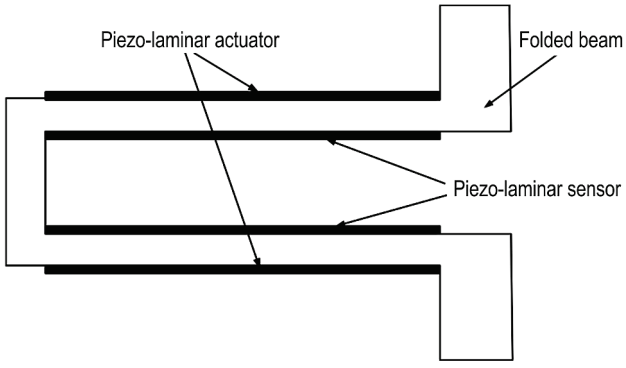

Figure 2 Cross section of piezoelectric folded beam

3 Finite element model

This active control platform is simplified as space frame structure and all the elements and nodes are numbered in Fig. 3. The figures in brackets are the elements' numbers and the others are the nodes'. Node 1 represents the centroid of RWA whose mass is assumed to be 10 kg and the moments of inertia are assumed to be I_{zz} = 0,08 kg·m^2 and I_{xx} = I_{yy} = 0,04 kg·m^2 being consistent with that in [13]. In this space frame, the vertical elements are normal space beam elements, the horizontal elements are piezoelectric beam elements which have piezoelectric layers glued on their upper and lower surfaces. The actuator and the sensor on the same beam have the same number and they are the actuator/sensor pair. The numbers of actuator/sensor pairs corresponding to the numbers of beams are shown in Tab. 1. All the sensor/actuator pairs are collocated for the maximum controllability [14, 15]. The nodes numbered 22, 23, 24 and 25 are fixed on the ground and their degrees of freedom (DOF) are restricted.

Table 1 Numbers of actuator/sensor pairs corresponding to beam

Object	Number							
Actuator/sensor pair	1	2	3	4	5	6	7	8
Beam	5	6	7	8	13	14	15	16

3.1 Mass and stiffness matrix

Finite element model of the platform is described using space frame elements with six DOF for each node. All the beams of the model are developed based on Euler-Bernoulli theory [16]. Kattanhas presented the process to develop the mass and stiffness matrices for general space frame and MATLAB codes are provided in [17]. Neglecting the effects of piezoelectric materials, we can get the mass and stiffness matrices of this control platform by employing these codes and along the route presented by Kamesh [10]. The brief process for developing these matrices is presented in the following sections.

3.1.1 Normal beam elements

Every vertical beam in Fig. 3 is a normal beam element and has dimensions 5 × 20 × 5 mm. The displacement of each node for a beam element in local coordinate system can be expressed as [16]

$$\boldsymbol{q}_{\mathrm{el}}^{\mathrm{T}} = [u_1, v_1, w_1, \phi_{x1}, \varphi_{y1}, \theta_{z1}, u_2, v_2, w_2, \phi_{x2}, \varphi_{y2}, \theta_{z2}]. \quad (1)$$

The stiffness matrix $\boldsymbol{K}_{\mathrm{el}}$ and mass matrix $\boldsymbol{M}_{\mathrm{el}}$ of a beam element can be developed by employing software MATLAB and both of them are symmetric with dimension 12 × 12. The single element's mass matrix and stiffness matrix are generally described in local coordinate. For developing the integrated finite element model, they must be expressed in global coordinate system, which can be achieved by performing the rotation from local coordinate system using rotating matrix $\boldsymbol{T}$.

$$\boldsymbol{q}_{\mathrm{es}} = \boldsymbol{T}\boldsymbol{q}_{\mathrm{el}}, \tag{2}$$

$$\boldsymbol{K}_{\mathrm{es}} = \boldsymbol{T}^{\mathrm{T}}\boldsymbol{K}_{\mathrm{el}}\boldsymbol{T}, \tag{3}$$

$$\boldsymbol{M}_{\mathrm{es}} = \boldsymbol{T}^{\mathrm{T}}\boldsymbol{M}_{\mathrm{el}}\boldsymbol{T}, \tag{4}$$

where $\boldsymbol{T}$ is 12×12 block diagonal matrix with 4 sub-blocks of 3×3 rotation matrix. The complete space frame model of this control platform can be developed by assembling all the elements' mass and stiffness matrices according to the number shown in Fig. 3.

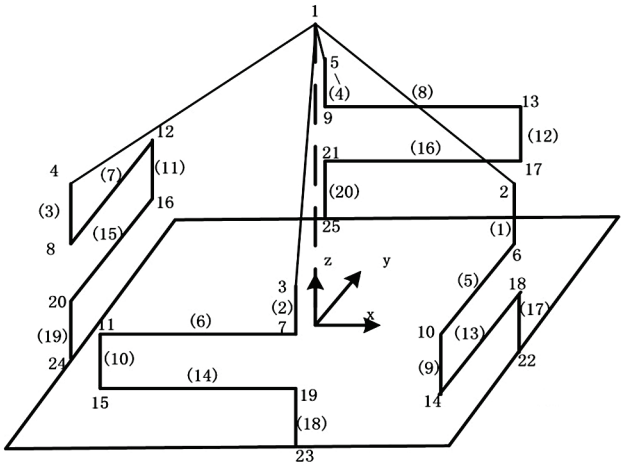

Figure3 The sketch of finite element model of control platform

The dimensions of global mass and stiffness matrices are 150 × 150. Constrains on nodes 22 ÷ 25 must be considered, which can be carried out by subtracting the rows and volumes on matrices corresponding to 22 ÷ 25 nodes. Nodes 2 ÷ 5 are connected rigidly to node 1, so the contribution from these four nodes' mass and stiffness matrices must be transferred to node 1 [10]. Finally add the contribution of RWA to the platform model and the final matrice achieved is 108 × 108. The primary dynamic equation is expressed as

$$\boldsymbol{M}_{\mathrm{es}}\ddot{\boldsymbol{q}}_{\mathrm{es}} + \boldsymbol{K}_{\mathrm{es}}\boldsymbol{q}_{\mathrm{es}} = \boldsymbol{F}, \tag{5}$$

where $\boldsymbol{q}_{\mathrm{es}}$ is displacement in global coordinate, and $\boldsymbol{F}$ is the external force.

3.1.2 Piezoelectric beam elements

In Fig. 3 the beam elements numbered as (5), (6), (7), (8), (13), (14), (15), and (16) with dimensions 55 × 20 × 7 mm are piezoelectric beam elements whose structure is shown in Fig. 4. The physical parameters of piezoelectric beam are given in Tab. 2.

In order to develop the mass and stiffness matrices of piezoelectric-beam element, the linear shape function N_u and cubic shape function N_w are used to get the strains of base beam and piezoelectric layer as

$$\left(\varepsilon_{xx}\right)_{\mathrm{b}} = \left(\varepsilon_{xx}(x,z,t)\right)_{\mathrm{b}} = \begin{bmatrix} N'_u & -zN''_w \end{bmatrix}\begin{Bmatrix} \overline{U} \\ \overline{W} \end{Bmatrix}, \tag{6}$$

$$\left(\varepsilon_{xx}\right)_{\mathrm{p}} = \left(\varepsilon_{xx}(x,z,t)\right)_{\mathrm{p}} = \begin{bmatrix} N'_u & -\left(\dfrac{h_{\mathrm{b}}}{2}+z\right)N''_w \end{bmatrix}\begin{Bmatrix} \overline{U} \\ \overline{W} \end{Bmatrix}, \tag{7}$$

here, $\overline{U}$ and $\overline{W}$ are the nodal DOFs [5, 10]. $\overline{U}$ is assumed to be the displacement along x axis, $\overline{W}$ includes the angular rotation around y axis and displacement along z axis in the local coordinate system.

The potential energy stored in a piezoelectric-beam is expressed as

$$U = U_{E_{\mathrm{b}}} + U_{E_{\mathrm{p}}} = \frac{1}{2}b\int_0^L\int_{-\frac{h_{\mathrm{p}}}{2}}^{\frac{h_{\mathrm{p}}}{2}}\left(E(x,z)(\varepsilon_{xx}(x,z,t))^2\right)\mathrm{d}z\mathrm{d}x, \tag{8}$$

where $U_{E\mathrm{b}}$ and $U_{E\mathrm{p}}$ are strain energies of base beam and piezoelectric layer elements respectively. These potential energy terms contribute to the stiffness matrix which is given as:

$$\boldsymbol{K}_{E_{\mathrm{b}}} = bE_{\mathrm{b}}\int_0^L\int_{-\frac{h_{\mathrm{b}}}{2}}^{\frac{h_{\mathrm{b}}}{2}}\begin{bmatrix} \{N'_u\}^{\mathrm{T}}\{N'_u\} & -z\{N'_u\}^{\mathrm{T}}\{N''_w\} \\ -z\{N''_w\}^{\mathrm{T}}\{N'_u\} & z^2\{N''_w\}^{\mathrm{T}}\{N''_w\} \end{bmatrix}\mathrm{d}z\mathrm{d}x, \tag{9}$$

$$\begin{aligned}\boldsymbol{K}_{E_{\mathrm{p}}} = {} & bE_{\mathrm{p}}\int_0^L\int_{-\frac{h_{\mathrm{b}}}{2}}^{\frac{h_{\mathrm{b}}}{2}+h_{\mathrm{p}}}\begin{bmatrix} \{N'_u\}^{\mathrm{T}}\{N'_u\} & -\left(\dfrac{h_{\mathrm{b}}}{2}+z\right)\{N'_u\}^{\mathrm{T}}\{N''_w\} \\ -\left(\dfrac{h_{\mathrm{b}}}{2}+z\right)\{N''_w\}^{\mathrm{T}}\{N'_u\} & \left(\dfrac{h_{\mathrm{b}}}{2}+z\right)^2\{N''_w\}^{\mathrm{T}}\{N''_w\} \end{bmatrix}\mathrm{d}z\mathrm{d}x + \\ & + bE_{\mathrm{p}}\int_0^L\int_{-\frac{h_{\mathrm{b}}}{2}-h_{\mathrm{p}}}^{\frac{h_{\mathrm{b}}}{2}}\begin{bmatrix} \{N'_u\}^{\mathrm{T}}\{N'_u\} & -\left(\dfrac{h_{\mathrm{b}}}{2}+z\right)\{N'_u\}^{\mathrm{T}}\{N''_w\} \\ -\left(\dfrac{h_{\mathrm{b}}}{2}+z\right)\{N''_w\}^{\mathrm{T}}\{N'_u\} & \left(\dfrac{h_{\mathrm{b}}}{2}+z\right)^2\{N''_w\}^{\mathrm{T}}\{N''_w\} \end{bmatrix}\mathrm{d}z\mathrm{d}x.\end{aligned} \tag{10}$$

In the above equations E_{b} and E_{p} are the modulus of base beam and piezo-layers, h_{b} and h_{p} are their thickness as shown in Fig. 4.

The complete stiffness matrix of piezoelectric beam element can be achieved by summarizing the stiffness matrix of base beam and the piezoelectric layers':

$$\boldsymbol{K}_{\mathrm{pl}} = \boldsymbol{K}_{E_{\mathrm{b}}} + \boldsymbol{K}_{E_{\mathrm{p}}}. \tag{11}$$

The total kinetic energy of a piezoelectric beam element can be expressed as:

$$T(t) = \frac{1}{2}b\int_0^L\int_{-\frac{b}{2}}^{\frac{b}{2}}\rho(x,z)\left((\dot{W}(x,z,t))^2 + (\dot{U}(x,z,t))^2\right)\mathrm{d}z\mathrm{d}x, \tag{12}$$

which includes three components, the kinetic energy associated with the transverse motion of the complete element T_W, the longitudinal motion $T_{U_{\mathrm{b}}}$ of base beam, and the longitudinal motion $T_{U_{\mathrm{p}}}$ of piezoelectric layers:

$$T = T_W + T_{U_{\mathrm{b}}} + T_{U_{\mathrm{p}}}. \tag{13}$$

The correspondent mass matrices can be assembled from the above kinetic energy equation:

$$\boldsymbol{M}_W = b(\rho_\mathrm{b} h_\mathrm{b} + \rho_\mathrm{p} h_\mathrm{p}) \int_0^L \begin{bmatrix} [0] & [0] \\ [0] & \{N_W\}^\mathrm{T}\{N_W\} \end{bmatrix} \mathrm{d}x, \tag{14}$$

$$\boldsymbol{M}_{u_\mathrm{b}} = b\rho_\mathrm{b} \int_0^L \int_{-\frac{h_\mathrm{b}}{2}}^{\frac{h_\mathrm{b}}{2}} \begin{bmatrix} \{N'_u\}^\mathrm{T}\{N'_u\} & -z\{N'_u\}^\mathrm{T}\{N''_w\} \\ -z\{N''_w\}^\mathrm{T}\{N'_u\} & z^2\{N''_w\}^\mathrm{T}\{N''_w\} \end{bmatrix} \mathrm{d}z\mathrm{d}x, \tag{15}$$

$$\boldsymbol{M}_{u_\mathrm{p}} = b\rho_\mathrm{p} \int_0^L \int_{-\frac{h_\mathrm{b}}{2}}^{\frac{h_\mathrm{b}}{2}+h_\mathrm{p}} \begin{bmatrix} \{N'_u\}^\mathrm{T}\{N'_u\} & -\left(\frac{h_\mathrm{b}}{2}+z\right)\{N'_u\}^\mathrm{T}\{N''_w\} \\ -\left(\frac{h_\mathrm{b}}{2}+z\right)\{N''_w\}^\mathrm{T}\{N'_u\} & \left(\frac{h_\mathrm{b}}{2}+z\right)^2\{N''_w\}^\mathrm{T}\{N''_w\} \end{bmatrix} \mathrm{d}z\mathrm{d}x + b\rho_\mathrm{p} \int_0^L \int_{-\frac{h_\mathrm{b}}{2}-h_\mathrm{p}}^{\frac{h_\mathrm{b}}{2}} \begin{bmatrix} \{N'_u\}^\mathrm{T}\{N'_u\} & -\left(\frac{h_\mathrm{b}}{2}+z\right)\{N'_u\}^\mathrm{T}\{N''_w\} \\ -\left(\frac{h_\mathrm{b}}{2}+z\right)\{N''_w\}^\mathrm{T}\{N'_u\} & \left(\frac{h_\mathrm{b}}{2}+z\right)^2\{N''_w\}^\mathrm{T}\{N''_w\} \end{bmatrix} \mathrm{d}z\mathrm{d}x, \tag{16}$$

where ρ_b and ρ_p are the densities of base beam and piezo-layers. These expressions lead to the following element mass matrix:

$$\boldsymbol{M}_{p1} = \boldsymbol{M}_W + \boldsymbol{M}_{u_\mathrm{b}} + \boldsymbol{M}_{u_\mathrm{p}}. \tag{17}$$

The displacements on the other DOF must be considered too. We make character $\overline{\phi}$ represent the angular rotating around x axis, $\overline{\theta}$ includes the displacement along y axis and the angular rotating around z axis. In the same manner as above, the mass matrix $\boldsymbol{M}_{\mathrm{p}2}$ and stiffness matrix $\boldsymbol{K}_{\mathrm{p}2}$ corresponding to these DOF can be achieved. It is assumed that $\boldsymbol{U}_1 = \left[\overline{U}^\mathrm{T} \quad \overline{W}^\mathrm{T}\right]^\mathrm{T}$ and $\boldsymbol{U}_2 = \left[\overline{\phi}^\mathrm{T} \quad \overline{\theta}^\mathrm{T}\right]^\mathrm{T}$. Two 12×6 transforming matrices $\boldsymbol{T}_1$ and $\boldsymbol{T}_2$ are used to assemble the nodal displacement $\boldsymbol{U}_1$ and $\boldsymbol{U}_2$ to a 12×1 complete displacement vector $\boldsymbol{q}_\mathrm{el}$

$$\boldsymbol{T}_1\boldsymbol{U}_1 + \boldsymbol{T}_2\mathrm{U}_2 = \boldsymbol{q}_\mathrm{el}. \tag{18}$$

The complete matrices of stiffness and mass are also assembled as:

$$\boldsymbol{K}_\mathrm{p} = \boldsymbol{T}_1\boldsymbol{K}_{\mathrm{p}1}\boldsymbol{T}_1^\mathrm{T} + \boldsymbol{T}_2\boldsymbol{K}_{\mathrm{p}2}\boldsymbol{T}_2^\mathrm{T}, \tag{19}$$

$$\boldsymbol{M}_\mathrm{p} = \boldsymbol{T}_1\boldsymbol{M}_{\mathrm{p}1}\boldsymbol{T}_1^\mathrm{T} + \boldsymbol{T}_2\boldsymbol{M}_{\mathrm{p}2}\boldsymbol{T}_2^\mathrm{T}. \tag{20}$$

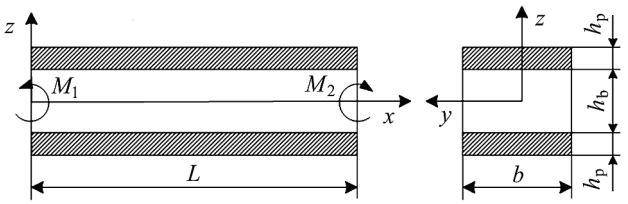

Figure 4 Figure of horizontal beam with piezoelectric layer

Table 2 Parameters of piezoelectric beam

Parameters of base beam				Parameters of piezoelectric material					
Thickness	Elastic modulus	Rigid modulus	Density	Elastic modulus	Density	Piezoelectric coefficient	Length	Width	Thickness
h_b	E_b	G_b	ρ_b	E_p	ρ_p	d_{31}	L	b	h_p
0,005 m	73,1 GPa	30 GPa	2790 kg/m^3	109,9 GPa	7800 kg/m^3	320×10^{-12} m/V	0,055 m	0,02 m	0,001 m

Transform the stiffness and mass matrices in Eqs. (19) and (20) from local coordinate to global coordinate, and replace them to the normal mass and stiffness matrices on the corresponding locations of global matrices. We can get the complete equation of motion for the platform with RWA as

$$\boldsymbol{M}\ddot{\boldsymbol{x}}(t) + \boldsymbol{L}\dot{\boldsymbol{x}}(t) + \boldsymbol{K}\boldsymbol{x}(t) = \boldsymbol{B}_0\boldsymbol{u}, \tag{21}$$

where $\boldsymbol{M}$, $\boldsymbol{L}$ and $\boldsymbol{K}$ are mass, damping and stiffness matrices and x, $\dot{x}$ and $\ddot{x}$ are the nodal displacement, nodal velocity and nodal acceleration. $\boldsymbol{B}_0$ is the external force location matrix and $\boldsymbol{u}$ is the force vector respectively. Damping matrix L is assumed to be a linear combination of stiffness and mass matrices as $\boldsymbol{L} = \alpha\boldsymbol{K} + \beta\boldsymbol{M}$, whith α and β being nonnegative scalars.

3.2 Piezoelectric Sensors

The linear piezoelectric coupling between the elastic field and the electric field can be expressed as equations below [3, 5]:

$$D_i = d_{ip}\sigma_p + e_{ij}^\sigma E_j \tag{22}$$

$$\varepsilon_p = s_{pq}^E\sigma_q + d_{pi}E_i \tag{23}$$

where D, σ, ε, E and d are electric displacement, stress, stain, electric field and piezoelectric constant, respectively e_{ij}^σ is dielectric constant at constant stress, S^E is the compliance coefficients matrix of piezoelectric material under constant dielectric displacement ($D = 0$). $i, j = 1, 2, 3$; $p, q = 1, 2, \ldots, 6$.

It is assumed polarization is done along the thickness (z-direction) of the sensors. When strain ε_x arises along the length (x-direction) of sensors, the electric displacement is

$$H_z = d_{31}E_\mathrm{p}\varepsilon_x = e_{31}\varepsilon_x. \tag{24}$$

The current output i from the piezoelectric sensor is

$$i(t) = \frac{\mathrm{d}Q(t)}{\mathrm{d}t} = \frac{\mathrm{d}}{\mathrm{d}t}\int H_z\mathrm{d}A = \frac{\mathrm{d}}{\mathrm{d}t}\int e_{31}\varepsilon_x\mathrm{d}A. \tag{25}$$

There is a relationship between the strain ε_x and displacement W as

$$\varepsilon_x = -\frac{\mathrm{d}^2W}{\mathrm{d}x^2}. \tag{26}$$

Thus the equation of current in Eq. (25) can be rewritten as

$$i(t)=\frac{\mathrm{d}Q(t)}{\mathrm{d}t}=-\int e_{31}N_w''\frac{\mathrm{d}}{\mathrm{d}t}(\overline{W})\mathrm{d}A. \tag{27}$$

This current can be converted into the open circuit voltage V^S for the convenience of measurement as

$$V^S(t)=-G_c e_{31} z b\int_0^L N_w''\frac{\mathrm{d}}{\mathrm{d}t}(\overline{W})\mathrm{d}x, \tag{28}$$

where $z=\frac{h_\mathrm{b}}{2}+h_\mathrm{p}$, G_c is the signal conditioning gain. So the final form of the sensor output voltage for beam element can be written as

$$V^s(t)=\begin{bmatrix}0 & G_c e_{31} z b & 0 & -G_c e_{31} z b\end{bmatrix}\left\{\ddot{\overline{W}}\right\}. \tag{29}$$

3.3 Piezoelectric actuators

The actuator equation can be derived from the converse piezoelectric equation [3]. Applying electric field E_f on actuator layer, the strain generated is given by

$$\varepsilon_x=d_{31}E_f \tag{30}$$

where

$$E_f=\frac{V^\mathrm{a}(t)}{h_\mathrm{p}}. \tag{31}$$

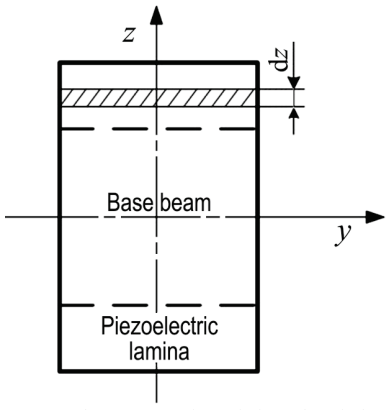

Figure 5 The cross section of piezoelectric beam

It is assumed that a small part of the beam's cross section is extracted from the entirety along the depth of the beam as shown in Fig. 5. Based on the equilibrium principle, the moment developed on this subsection can be expressed as

$$\mathrm{d}M=-E_\mathrm{p}I_\mathrm{p}\frac{\mathrm{d}^2W}{\mathrm{d}x^2}. \tag{32}$$

Substitute Eq. (26) for (32) to get the relationship between developed moment dM and stress σ_a as

$$\mathrm{d}M=I_\mathrm{p}\frac{\sigma_x}{z}. \tag{33}$$

Integrate Eq. (33) to the whole thickness to get the moment acting on the cross section of beam element as

$$M(t)=\int_{\frac{h_\mathrm{b}}{2}}^{h_\mathrm{p}+\frac{h_\mathrm{b}}{2}} I_\mathrm{p}\frac{\sigma_\mathrm{a}}{z}\mathrm{d}z=bE_\mathrm{p}d_{31}\bar{z}V^\mathrm{a}(t), \tag{34}$$

where $\bar{z}=\frac{h_\mathrm{b}}{2}+h_\mathrm{p}$.

Based on the relationship between strain and moment the force along the x-axis direction in Fig. 4 can be achieved.

$$F=S\sigma_\mathrm{a}=bE_\mathrm{p}d_{31}V^\mathrm{a}(t), \tag{35}$$

where S is the cross section area of piezoelectric lamina. In position x on the x-axis of beam element, the component of F along z-axis direction is given as

$$F_1=FW'(x,t)=bE_\mathrm{p}d_{31}V^\mathrm{a}(t)W'(x,t). \tag{36}$$

The control force generated by the piezoelectric actuator is the integration of F_1 through the x-axis as

$$F_\mathrm{ctrl}=bE_\mathrm{p}d_{31}\bar{z}\int N'_W\,\mathrm{d}xV^\mathrm{a}(t)=hV^\mathrm{a}(t), \tag{37}$$

where

$$h^\mathrm{T}=\begin{bmatrix}-bE_\mathrm{p}d_{31}\bar{z} & 0 & bE_\mathrm{p}d_{31}\bar{z} & 0\end{bmatrix}. \tag{38}$$

4 Dynamic analysis of active control platform

4.1 Modal analysis of control platform

The finite element model of active control platform is developed in software ANSYS as is shown in Fig. 6 with element meshing and numbering the same as in Fig. 3. In this model, BEAM4 elements are used to describe all the beams. The vertical ones are normal aluminium beams, but the horizontal beams include aluminium and piezoelectric materials. So these elements' properties must include the effect of piezoelectric material. The beam elements 17, 18, 19, and 20 are constrained in the nether nodes by setting their DOF to zero. Node 25 represents the centroid of the RWA which is described by the element MASS21 in ANSYS and has the same mass and moments of inertia as mentioned in subsection 3.3. The top nodes of the four folded beams are connected with node 25 by rigid element MPCs which are numbered as 21, 22, 23 and 24. The properties of all the elements in the model preserve uniformity with what is shown in Tab. 2. The first six steps modal frequencies from ANSYS and Eq. (21) are given in Tab. 3.

Two pairs of reduplicate frequencies are existent as a result of the symmetry of platform. The frequency values in each pair keep the same and share the same mode. The first and the second step frequencies correspond to the rock mode while the third keeps consistent to the vertical translation mode, the forth to the torsion mode, the fifth and the sixth correspond to the horizontal translation mode. To simplify this issue, we combine the first and the second modals as a new one, the fifth and the sixth modals as another. The two new modal vectors are normalized and used to constitute the base vectors of modal space with the residual two. The control system is designed in this new modal space.

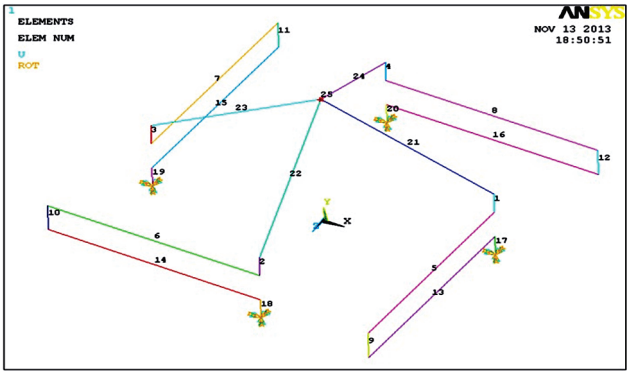

Figure 6 Finite element model of control platform in ANSYS

Table 3 Modal frequency from ANSYS and dynamic equation

Step/Mode		Frequency (Hz)	
		ANSYS	Dynamic equation
1	Rock	45,93	46,01
2		45,93	46,01
3	Vertical translation	76,34	76,28
4	Torsion	123,81	123,29
5	Horizontal translation	197,82	197,90
6		197,82	197,90

4.2 Model reduction

As a summary of the calculations above, the complete model including active control platform and RWA can be expressed as

$$\boldsymbol{M}\ddot{\boldsymbol{q}} + \boldsymbol{K}\boldsymbol{q} = \boldsymbol{B}_f\boldsymbol{U}_f + \boldsymbol{B}_c\boldsymbol{U}_f = \boldsymbol{F}_{\text{ext}} + \boldsymbol{F}_{\text{ctrl}}. \tag{39}$$

Where $\boldsymbol{K}$ and $\boldsymbol{M}$ are stiffness and mass matrices, $\boldsymbol{q}$ and $\ddot{\boldsymbol{q}}$ are vectors of displacement and acceleration of nodes, $\boldsymbol{U}_f$ and $\boldsymbol{U}_C$ are the disturbances and controlling force vectors, $\boldsymbol{B}_f$ and $\boldsymbol{B}_c$ are inputting matrices of disturbances and controlling force. For designing the controller, model reduction must be performed and we reserve only the first six modes. At first, the dimension of modal matrix $\boldsymbol{\Phi}$ whose volumes are the modal vectors is chosen as $n_d \times 4$ based on the results of modal analysis, and then transform the dynamic model into modal space by employing modal matrix $\boldsymbol{\Phi}$:

$$\boldsymbol{\Phi}^{\mathrm{T}}\boldsymbol{M}\boldsymbol{\Phi}\ddot{\boldsymbol{z}} + \boldsymbol{\Phi}^{\mathrm{T}}\boldsymbol{K}\boldsymbol{\Phi}\boldsymbol{z} = \boldsymbol{\Phi}^{\mathrm{T}}\boldsymbol{F}_{\text{ext}} + \boldsymbol{\Phi}^{\mathrm{T}}\boldsymbol{F}_{\text{ctrl}}, \tag{40}$$

which can be simplified as

$$\boldsymbol{M}_{\mathrm{m}}\ddot{\boldsymbol{z}} + \boldsymbol{K}_{\mathrm{m}}\boldsymbol{z} = \boldsymbol{F}^*_{\text{ext}} + \boldsymbol{F}^*_{\text{ctrl}}. \tag{41}$$

The modal damping matrix $\boldsymbol{L}_{\mathrm{m}} = \beta\boldsymbol{M}_{\mathrm{m}} + \alpha\boldsymbol{K}_{\mathrm{m}}$ mentioned before must be introduced into Eq. (41) and the complete dynamic equation of structure can be rewritten as

$$\boldsymbol{M}_{\mathrm{m}}\ddot{\boldsymbol{z}} + \boldsymbol{L}_{\mathrm{m}}\dot{\boldsymbol{z}} + \boldsymbol{K}_{\mathrm{m}}\boldsymbol{z} = \boldsymbol{F}^*_{\text{ext}} + \boldsymbol{F}^*_{\text{ctrl}}, \tag{42}$$

which can be transformed to the state-space form as

$$\dot{\boldsymbol{x}} = \boldsymbol{A}\boldsymbol{x} + \boldsymbol{B}\boldsymbol{u}, \tag{43}$$

where $\boldsymbol{u}$ is the input matrix and

$$\boldsymbol{A} = \begin{bmatrix} 0 & \boldsymbol{I} \\ -\boldsymbol{M}_{\mathrm{m}}^{-1}\boldsymbol{K}_{\mathrm{m}} & -\boldsymbol{M}_{\mathrm{m}}^{-1}\boldsymbol{L}_{\mathrm{m}} \end{bmatrix}_{8\times 8}, \tag{44}$$

$$\boldsymbol{B} = \begin{bmatrix} 0 \\ \boldsymbol{M}_{\mathrm{m}}^{-1}\boldsymbol{\Phi}^{\mathrm{T}}\boldsymbol{h} \end{bmatrix}_{8\times 8}. \tag{45}$$

In Eq. (45) $\boldsymbol{h}$ is a constant matrix which represents the actuators' location on the space frame and their characteristic properties with dimension $n_d \times 8$ where 8 is the number of actuators. The output equation is

$$y(t) = Cx(t) \tag{46}$$

where

$$\boldsymbol{C} = \begin{bmatrix} 0 & \boldsymbol{P}^{\mathrm{T}}\boldsymbol{\Phi} \end{bmatrix}. \tag{47}$$

Matrix $\boldsymbol{P}$ is also constant and represents the location on the frame and characteristic properties of sensors with dimensions $n_d \times 8$.

5 Active control simulation

5.1 Active control system model

As we have built the active control platform's model, the next step is to choose appropriate control method. The voltage applied to the actuator can be determined by different control laws based on the sensing signal. Regular methods include velocity feedback, displacement feedback, model predictive control [18], linear Quadratic Gaussian (LQG) optimal control and others [19]. The LQG method requires an observer to estimate the states which would rise the risk of failure and is complicated for using. The output feedback control scheme is relatively simple and provides higher reliability and stability [12]. Thus, periodic output feedback (POF) control is implemented for controller design here.

Consider a LTI continuous time system [5]:

$$\dot{\boldsymbol{x}} = \boldsymbol{A}\boldsymbol{x} + \boldsymbol{B}\boldsymbol{u}, \quad \boldsymbol{y} = \boldsymbol{C}\boldsymbol{x}. \tag{48}$$

Let $(\boldsymbol{\Phi}_\tau, \boldsymbol{\Gamma}_\tau, \boldsymbol{C})$ and $(\boldsymbol{\Phi}, \boldsymbol{\Gamma}, \boldsymbol{C})$ be the system sampled at τ and Δ seconds, and they are named τ system and Δ system respectively. It is assumed that τ system is

completed observable and Δ system is completed controllable. The output is measured at $t = k\tau$, $k = 0, 1, 2, \ldots$. An output-sampling interval is divided into N sub-intervals of width $\Delta = \tau/N$ and a constant hold function is used between the two adjacent sub-intervals. N should be greater than the controllability index of $(\boldsymbol{\Phi}_\tau, \boldsymbol{\Gamma})$. The control law becomes:

$$u(t) = K_1 y(k\tau) \tag{49}$$

where $k\tau + l\Delta \le t \le k\tau + (l+1)\Delta$, $l = 0,1,2,\ldots,(N-1)$ and $K_{1+N} = K_1$. So the key of POF control is the determination of gain matrix $\boldsymbol{K}$.

$$\boldsymbol{K} = \begin{bmatrix} K_0 & K_1 & \cdots & K_{N-1} \end{bmatrix}^{\mathrm{T}}. \tag{50}$$

Consider the Δ system

$$\boldsymbol{x}(k+1) = \boldsymbol{\Phi}\boldsymbol{x}(k) + \boldsymbol{\Gamma}\boldsymbol{u}(k), \qquad \boldsymbol{y}(k) = \boldsymbol{C}\boldsymbol{x}(k). \tag{51}$$

The input $\boldsymbol{u}(t)$ has the form as

$$\boldsymbol{U}(k\tau) = \boldsymbol{K}y(k\tau) = \begin{bmatrix} u(k\tau) \\ u(k\tau+\Delta) \\ \vdots \\ u(k\tau+\tau-\Delta) \end{bmatrix}. \tag{52}$$

The τ system is written as

$$\boldsymbol{x}(k\tau+\tau) = \boldsymbol{\Phi}^N \boldsymbol{x}(k\tau) + \boldsymbol{\Gamma}_\tau \boldsymbol{U}(k\tau); \; \boldsymbol{y}(k\tau) = \boldsymbol{C}\boldsymbol{x}(k\tau), \tag{53}$$

where $\boldsymbol{\Gamma}_\tau = \begin{bmatrix} \Phi^{N-1}\Gamma & \Phi^{N-2}\Gamma & \cdots & \Gamma \end{bmatrix}$.

Applying the control in Eq. (52), $\boldsymbol{K}y(k\tau)$ is substituted for $\boldsymbol{U}(k\tau)$, then the closed loop system becomes:

$$\boldsymbol{x}(k\tau+\tau) = (\boldsymbol{\Phi}^N + \boldsymbol{\Gamma}_\tau \boldsymbol{K}\boldsymbol{C})\boldsymbol{x}(k\tau). \tag{54}$$

In order to get the best gain matrix $\boldsymbol{K}$, a performance index $\boldsymbol{J}(k)$ is given by:

$$J(k) = \sum_{l=0}^{\infty} \begin{bmatrix} x_l^{\mathrm{T}} & u_l^{\mathrm{T}} \end{bmatrix} \begin{bmatrix} Q & 0 \\ 0 & R \end{bmatrix} \begin{bmatrix} x_l \\ u_l \end{bmatrix} + \\ + \sum_{k=1}^{\infty} (x_{kN} - x_{kN}^*)^{\mathrm{T}} P (x_{kN} - x_{kN}^*), \tag{55}$$

where $\boldsymbol{Q}$, $\boldsymbol{R}$ and $\boldsymbol{P}$ are positive definite and symmetric weighting matrices with proper dimensions. x_l and u_l are the states and the inputs of the delta system respectively, x_{kN}^* denotes the state that would be reached at the instant kN. The first term in Eq. (55) represents 'averaged' state and control energy whereas the second term penalizes the deviation of $\boldsymbol{K}$.

5.2 Disturbances analysis

Many studies have investigated the disturbances produced by RWA [20 ÷ 23]. It is concluded that disturbances arise from four main sources: flywheel imbalance, mechanical bearing noise, motor drive errors, and motor disturbances. Generally flywheel imbalance is considered to be the largest disturbance source [12].

The disturbances of RWA are harmonic and their frequencies are proportional to the rotating speed of the flywheel. Because of the elasticity of structure, there are three existing modes, namely translational mode, axial mode and rock mode. These modes are consistent with control platform' modes mentioned before. For RWA there are two components in the rock mode, the positive procession and the inverse procession, whose frequencies are related to the rotating speed of flying wheel. When the frequency of disturbance is near the natural frequencies of RWA, the amplitudes of vibration will be amplified [13]. When RWA is mounted on the control platform, the whole structure's natural frequencies contribute to the disturbances. Once the resonances are restrained, the disturbances' effects are controlled efficiently. In order to emphasize the effects of RWA's natural frequencies to disturbances, white noises as input are selected as the disturbance here.

5.3 Simulation results and discussion

To complete the control system design we choose the coefficients in damping matrix as α = 0,0005 and β = 0,0002. Weighting matrices of the control method are chosen as $\boldsymbol{Q} = 10^{12}\boldsymbol{I}_8$ and $\boldsymbol{R} = 0{,}5\boldsymbol{I}_8$, where $\boldsymbol{I}$ is the identity matrix. The final coefficient matrices in state space equation (Eq. 48) can be achieved as

$$\boldsymbol{A} = \begin{bmatrix} A_1 & A_2 \\ A_3 & A_4 \end{bmatrix}_{8\times 8}, \; A_1 = [0]_{4\times 4}, \; A_2 = [I]_{4\times 4},$$

$$A_3 = \begin{bmatrix} -8{,}315\times10^4 & 0 & 0 & 0 \\ 0 & -1{,}092\times10^5 & 0 & 0 \\ 0 & 0 & -5{,}961\times10^5 & 0 \\ 0 & 0 & 0 & -1{,}546\times10^6 \end{bmatrix},$$

$$A_4 = \begin{bmatrix} -16{,}63 & 0 & 0 & 0 \\ 0 & -21{,}84 & 0 & 0 \\ 0 & 0 & -119{,}23 & 0 \\ 0 & 0 & 0 & -309{,}25 \end{bmatrix},$$

$$\boldsymbol{B} = \begin{bmatrix} B_1 & B_2 \\ B_3 & B_4 \end{bmatrix}_{8\times 8}, \; B_1 = B_2 = [0]_{4\times 4},$$

$$B_3 = \begin{bmatrix} -2{,}05\times10^{-4} & -3{,}04\times10^{-4} & 2{,}05\times10^{-4} & 3{,}04\times10^{-4} \\ 3{,}55\times10^{-4} & -2{,}34\times10^{-4} & -3{,}55\times10^{-4} & 2{,}34\times10^{-4} \\ 7{,}73\times10^{-4} & 7{,}73\times10^{-4} & 7{,}73\times10^{-4} & 7{,}73\times10^{-4} \\ 9{,}57\times10^{-5} & -1{,}70\times10^{-3} & -9{,}57\times10^{-5} & 1{,}70\times10^{-3} \end{bmatrix},$$

$$B_4 = \begin{bmatrix} -2{,}07\times10^{-4} & 3{,}03\times10^{-4} & 2{,}07\times10^{-4} & -3{,}03\times10^{-4} \\ -3{,}55\times10^{-4} & -2{,}37\times10^{-4} & 3{,}55\times10^{-4} & 2{,}37\times10^{-4} \\ -7{,}64\times10^{-4} & -7{,}64\times10^{-4} & -7{,}64\times10^{-4} & -7{,}64\times10^{-4} \\ -8{,}36\times10^{-6} & 1{,}70\times10^{-3} & 8{,}36\times10^{-6} & -1{,}70\times10^{-3} \end{bmatrix},$$

$$\boldsymbol{C} = \begin{bmatrix} C_1 & C_2 \end{bmatrix}_{8\times 8},\ C_1 = [0]_{8\times 4},$$

$$B_4 = \begin{bmatrix} -4{,}97 & -0{,}0041 & -2{,}04 & 9{,}11 \\ -2{,}20 & -0{,}6900 & -10{,}17 & 23{,}39 \\ -4{,}97 & -0{,}0041 & 2{,}04 & 9{,}11 \\ -2{,}20 & -0{,}6900 & 10{,}17 & 23{,}39 \\ -5{,}16 & -0{,}0043 & 2{,}04 & -6{,}96 \\ -2{,}72 & -0{,}6900 & 10{,}19 & -22{,}31 \\ -5{,}16 & -0{,}0043 & 2{,}04 & -6{,}96 \\ -2{,}72 & -0{,}6900 & 10{,}19 & -22{,}31 \end{bmatrix}.$$

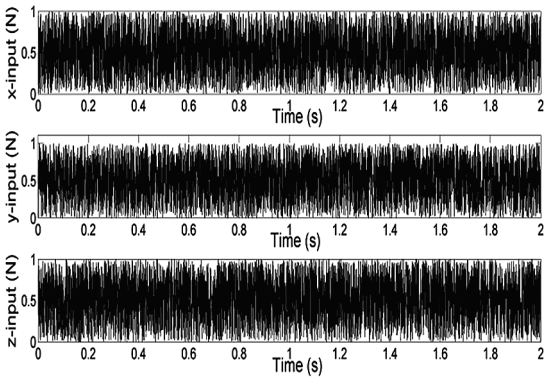

Figure 7 Random signals input to the *x*, *y*, *z* directions

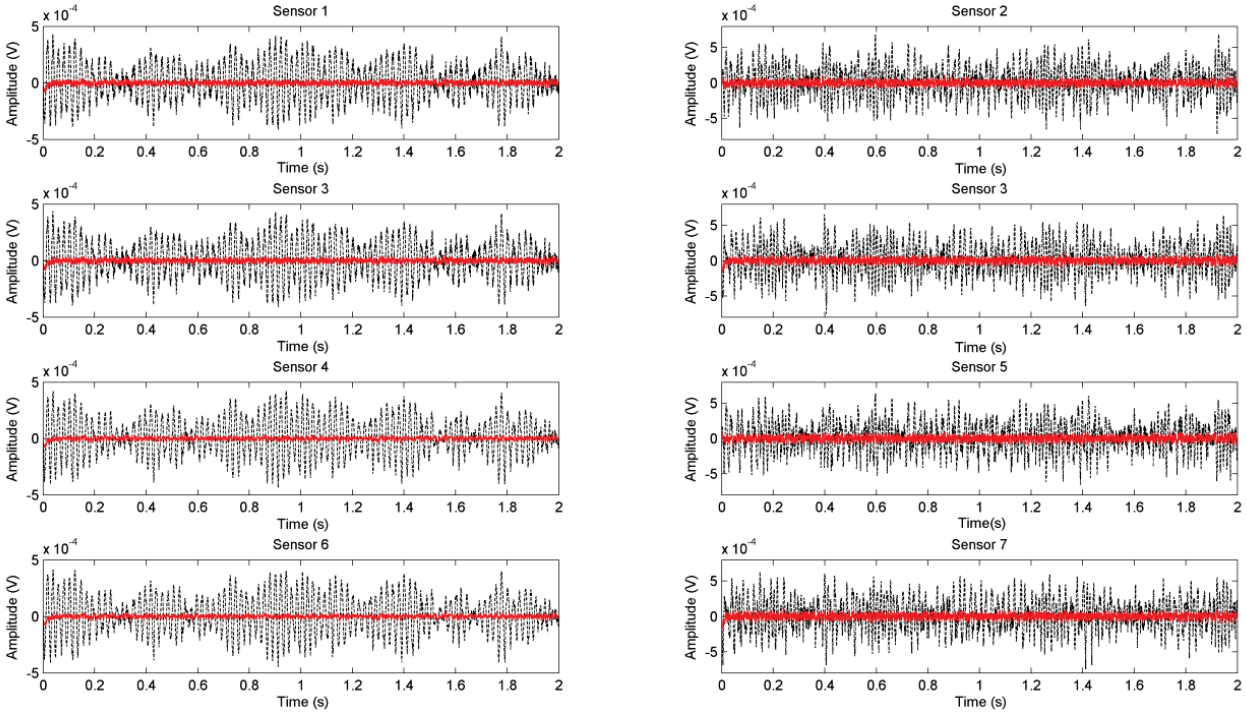

Figure 8 The comparison of uncontrolled and controlled vibration levels measured from eight sensors (---uncontrolled response, —controlled response)

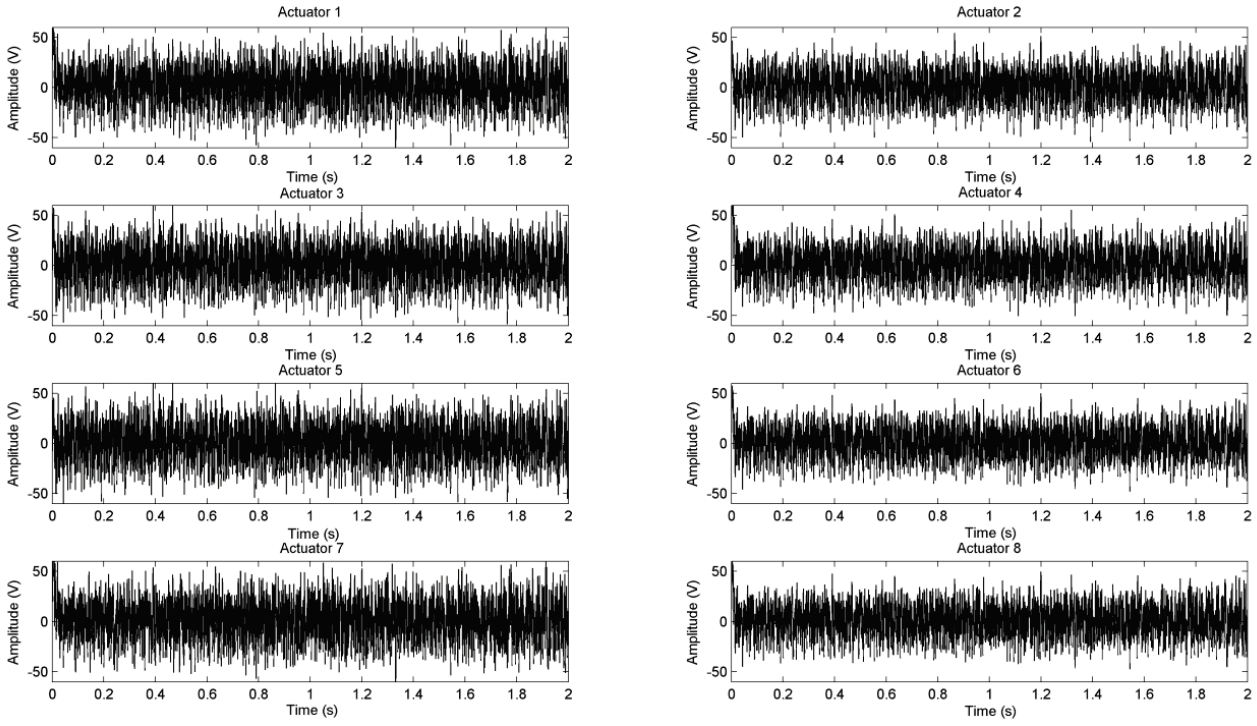

Figure 9 Control input to the eight actuators under the white noise disturbances to system

Three random disturbances which are generated from the MATLAB function RANDON are applied to this system, which includes active control platform and RWA, on node 1 along 1 ÷ 3 DOF (x, y, z-directions). These disturbances are shown in Fig. 7. Keep active control on in the simulation, and the responses from all the eight sensors are measured and recorded. The controlled and uncontrolled responses are compared in Fig. 8. It can be concluded that the amplitudes of the sensors' responses decrease more than 20 dB when there is active control, which means the vibration level is attenuated effectively. Because the contributions from first six modes to vibration response are primary, once their amplitudes are controlled, the residual modes' effects can be neglected. The voltages applied on the eight piezoelectric actuators are recorded too, and Fig. 9 represents the voltages acted on the eight actuators, their amplitudes observed are all less than 50 V and within the PZT threshold.

6 Conclusion

A micro-vibration active control platform's design, modelling, and active control simulation have been presented in this paper. The piezoelectric folded beams with enough static stiffness to support RWA or CMG are designed for maximum controllability. The using of space frame elements makes the platform's modelling easy and the treatments in the modelling process are also suitable for other smart structures including beams.

In the active control simulation for this active control platform, the condition of random inputs simulating RWA's disturbance on the three directions have been studied. Numerical results indicate that the vibration due to the disturbance of RWA can be relieved significantly by equipping this active control platform. The amplitudes of vibration have decreased effectively more than 20 dB. It can be concluded this platform configured with folded beams is able to attenuate the micro-vibration for space use. In the future, the optimal design of the platform shape should be considered and more experiments should be set up to validate the control performance of this active control platform.

7 References

[1] Kamesh, D.; Pandiyan, R.; Ghosal, A. Passive vibration isolation of reaction wheel disturbances using a low frequency flexible space platform. // Journal of sound and Vibration. 331, 6(2012), pp. 1310-1330.

[2] Yiu, Y. C.; Regelbrugge, M. E. Shape-memory alloy isolators for vibration suppression in space applications. //American Institute of Aeronautics and Astronautics/ AIAA-95-1120-CP, 1995, pp. 3390-3398.

[3] Jalili, N. Piezoelectric-Based Vibration Control: from macro to micro/nano scale systems. New York: Springer Science Business Media, LLC, 2010. pp. 125-140.

[4] Wu, D. F.; Liu, A. C.; Mai, H. C. Study on active vibration control of piezoelectric intelligent flexible beam. // Journal of Beijing University of Aeronautics and Astronautics. 30, 2(2004), pp. 160-163 (in Chinese).

[5] Bandyopadhyay, B.; Manjunath, T. C.; Umapathy, M. Modeling, control and implementation of smart structures. New York: Springer-Verlag, 2007 .

[6] Manjunath, T. C.; Bandyopadhyay, B. Vibration control of a smart structure using periodic output feedback technique. // Asian Journal of Control. 6, 1(2004), pp. 74-87.

[7] Manjunath, T. C.; Bandyopadhyay, B. Control of vibration in flexible smart structures using fast output sampling feedback technique. // International Journal of Computational Intelligence. 3, 1(2006), pp. 127-141.

[8] Manjunath, T. C.; Bandyopadhyay, B. Controller design for Euler-Bernoulli smart structures using robust decentralized FOS via reduced order modelling. // International Journal of Computational Intelligence. 1, 2(2006), pp. 111-130.

[9] Hanagud, S.; Obal, M. W.; Callise, A. J. Optimal vibration control by the use of piezoceromic sensors and actuators // Journal of Guidance, Control, and Dynamics. 15, 5(1992), pp. 1199-1206.

[10] Kamesh, D.; Pandiyan, R.; Ghosal, A. Modeling, design and analysis of low frequency platform for attenuating micro-vibration in spacecraft. // Journal of Sound and Vibration. 329, 17(2010), pp. 3431-3450.

[11] Zhou, W. Y.; Aglietti, G. S.; Zhang, Z. Modelling and testing of a soft suspension design for a reaction/momentum wheel assembly. // Journal of Sound and Vibration. 330, 18(2011), pp. 4596-4610.

[12] Zhou, W. Y.; Li, D. X. Design and analysis of an intelligent vibration isolation platform for reaction/momentum wheel assemblies. // Journal of Sound and Vibration. 331, 13(2012), pp. 2984-3005.

[13] Wang, Y. F.; Cheng, W. Parameter Identification of Reaction Wheel Disturbance Model based WLS-SVR Method.// 4th International Conference on Information Technology for Manufacturing Systems / Auckland, 2013, pp.144-149.

[14] Wang, Q.; Wang, C.M. Optimal placement and size of piezoelectric patches on beams from the controllability perspective. // Smart Materials and Structures. 9, 4(2000), pp. 558-567.

[15] Preumont, A. Vibration control of active structures, an introduction. 2nd ed. Kluwer Academic Publishers, Netherlands, 2002.

[16] Weaver, W.; Johnston, P. R. Structural Dynamics by Finite elements. Prentice- Hall, Inc., New Jersey, 1987, pp. 73-108.

[17] Kattan, P. I. MATLAB Guide to Finite Element: An Interactive Approach. 2nd ed. Springer-Verlag, Heidelberg, 2008.

[18] Dubravić, A.; Šehić, Z. Using orthonormal functions in model predictive control. // Tehnički vjesnik/Technical Gazette. 19, 3(2012), pp. 513-520.

[19] Alkhatib, R.; Golnaraghi, M. F. Active structural vibration control: a review. // The Shock and Vibration Digest, 35, 5(2003), pp. 367-383.

[20] Narayan, S. S.; Nair, P. S.; Ghosal, A. Dynamic interaction of rotating momentum wheels with spacecraft elements. // Journal of Sound and Vibration. 315, 4(2008), pp. 970-984.

[21] Liu, K. C.; Maghami, P.; Blaurock, C. Reaction wheel disturbance modeling, jitter analysis, and validation tests for Solar Dynamics Observatory. // AIAA Guidance, Navigation and Control Conference and Exhibit / Honolulu, Hawaii, 2008, pp. 1-18.

[22] Bialke, B. A compilation of reaction wheel induced spacecraft disturbances.// 20th Annual AAS Guidance and Control Conference / 1997, Paper. 97-038.

[23] Masterson, R. A.; Miller, D. W. Development and Validation of Empirical and Analytical Reaction Wheel Disturbance Models. Master Thesis, Department of Mechanical Engineering, Massachusetts Institute of Technology, 1999.

Authors' addresses

Yun-Feng Wang, PhD student
School of Aeronautic Science and Engineering,
Beijing University of Aeronautics and Astronautics
Xue Yuan Road No. 37, Hai Dian District, Beijing, China
E-mail: wangyunfengdoc@126.com

Wei Cheng, Professor
School of Aeronautic Science and Engineering,
Beijing University of Aeronautics and Astronautics
XueYuan Road No. 37, Hai Dian District, Beijing, China
E-mail: cheng_wei@buaa.edu.cn